ARMY RESEARCH LABORATORY

CFD Computation of Magnus Moment and Roll Damping Moment of a Spinning Projectile

by James DeSpirito and Karen R. Heavey

ARL-RP-131 **September 2006**

A reprint from the *AIAA Atmospheric Flight Mechanics Conference and Exhibit,* Providence, RI, 16–19 August 2004.

NOTICES

Disclaimers

The findings in this report are not to be construed as an official Department of the Army position unless so designated by other authorized documents.

Citation of manufacturer's or trade names does not constitute an official endorsement or approval of the use thereof.

Destroy this report when it is no longer needed. Do not return it to the originator.

Army Research Laboratory
Aberdeen Proving Ground, MD 21005-5066

ARL-RP-131 **September 2006**

CFD Computation of Magnus Moment and Roll Damping Moment of a Spinning Projectile

James DeSpirito and Karen R. Heavey
Weapons and Materials Research Directorate, ARL

A reprint from the *AIAA Atmospheric Flight Mechanics Conference and Exhibit,*
Providence, RI, 16–19 August 2004.

REPORT DOCUMENTATION PAGE

Form Approved
OMB No. 0704-0188

1. REPORT DATE *(DD-MM-YYYY)*	2. REPORT TYPE	3. DATES COVERED (From - To)
September 2006	Reprint	July 2003–August 2004

4. TITLE AND SUBTITLE
CFD Computation of Magnus Moment and Roll Damping Moment of a Spinning Projectile

5a. CONTRACT NUMBER

5b. GRANT NUMBER

5c. PROGRAM ELEMENT NUMBER

6. AUTHOR(S)
James DeSpirito and Karen R. Heavey

5d. PROJECT NUMBER
1L1626I8AH80

5e. TASK NUMBER

5f. WORK UNIT NUMBER

7. PERFORMING ORGANIZATION NAME(S) AND ADDRESS(ES)
U.S. Army Research Laboratory
ATTN: AMSRD-ARL-WM-BC
Aberdeen Proving Ground, MD 21005-5066

8. PERFORMING ORGANIZATION REPORT NUMBER
ARL-RP-131

9. SPONSORING/MONITORING AGENCY NAME(S) AND ADDRESS(ES)

10. SPONSOR/MONITOR'S ACRONYM(S)

11. SPONSOR/MONITOR'S REPORT NUMBER(S)

12. DISTRIBUTION/AVAILABILITY STATEMENT
Approved for public release; distribution is unlimited.

13. SUPPLEMENTARY NOTES
A reprint from the *AIAA Atmospheric Flight Mechanics Conference and Exhibit*, 16–19 August 2004, Providence, RI.

14. ABSTRACT

Computational fluid dynamic simulations (CFD) were used to predict the aerodynamic coefficients and flow field over a spin-stabilized, 25-mm, sub-caliber training projectile. The primary objective of the investigation was to determine the CFD parameters necessary for the accurate prediction of the Magnus moment and roll damping of a spin-stabilized projectile. Archival experimental data was used to validate the numerical calculations. The Mach number range investigated was from 0.4 to 4.5. Steady state CFD calculations predicted the drag, normal force, pitching moment, and normal force center of pressure very well—to within 10% of the experimental data. Time-accurate, detached-eddy simulations were found necessary to predict the Magnus moment in the subsonic and transonic flow regimes. Steady state CFD was found adequate to calculate the roll damping, which was predicted to within 15% of the experimental data in both steady state and time accurate calculations.

15. SUBJECT TERMS
aerodynamics, computational fluid dynamics, Magnus, roll-damping

16. SECURITY CLASSIFICATION OF:			17. LIMITATION OF ABSTRACT	18. NUMBER OF PAGES	19a. NAME OF RESPONSIBLE PERSON
a. REPORT	b. ABSTRACT	c. THIS PAGE			James DeSpirito
UNCLASSIFIED	UNCLASSIFIED	UNCLASSIFIED	UL	24	19b. TELEPHONE NUMBER (*Include area code*) 410-278-6104

AIAA Atmospheric Flight Mechanics Conference and Exhibit
16 - 19 August 2004, Providence, Rhode Island

AIAA 2004-4713

CFD Computation of Magnus Moment and Roll Damping Moment of a Spinning Projectile

James DeSpirito* and Karen R. Heavey†
U.S. Army Research Laboratory, Aberdeen Proving Ground, Maryland 21005-5066

Computational fluid dynamic simulations (CFD) were used to predict the aerodynamic coefficients and flow field over a spin-stabilized, 25-mm, sub-caliber training projectile. The primary objective of the investigation was to determine the CFD parameters necessary for the accurate prediction of the Magnus moment and roll damping of a spin-stabilized projectile. Archival experimental data was used to validate the numerical calculations. The Mach number range investigated was from 0.4 to 4.5. Steady state CFD calculations predicted the drag, normal force, pitching moment, and normal force center of pressure very well—to within 10% of the experimental data. Time-accurate, detached-eddy simulations were found necessary to predict the Magnus moment in the subsonic and transonic flow regimes. Steady state CFD was found adequate to calculate the roll damping, which was predicted to within 15% of the experimental data in both steady state and time accurate calculations.

Nomenclature

C_D	=	drag coefficient, (drag force /$q_\infty S$)
C_{D0}	=	zero-yaw drag coefficient
$C_{L\alpha}$	=	lift coefficient derivative, (lift force / $q_\infty S \sin \alpha$)
C_{lp}	=	roll damping coefficient, (roll moment / $q_\infty S d [p_s d / 2 U_\infty]$)
$C_{m\alpha}$	=	pitching moment coefficient derivative, (pitching moment / $q_\infty S d \sin \alpha$)
$C_{N\alpha}$	=	normal force coefficient derivative, (normal force / $q_\infty S \sin \alpha$)
C_{np}	=	Magnus moment coefficient, (Magnus moment / $q_\infty S d [p_s d / 2 U_\infty]$)
$C_{np\alpha}$	=	Magnus moment coefficient derivative, (Magnus moment / $q_\infty S d [p_s d / 2 U_\infty] \sin \alpha$)
C_p	=	pressure coefficient, $(p - p_\infty) / q_\infty$
$C_{Yp\alpha}$	=	Magnus force coefficient derivative, (Magnus force / $q_\infty S [p_s d / 2 U_\infty] \sin \alpha$)
d	=	missile base diameter, m
k	=	turbulence kinetic energy, m^2/s^2
M	=	Mach number
p	=	pressure, N/m^2
p_s	=	projectile spin rate, rad/s
q_∞	=	dynamic pressure, ($\frac{1}{2} \rho U_\infty^2$)
R	=	undamped eddy viscosity, m^2/s
S	=	projectile cross-sectional area, m^2
U_∞	=	freestream velocity, m/s
x, y, z	=	axial, horizontal, and vertical body axes
x_{cg}	=	center of gravity location
x_{cp}	=	normal force center of pressure location, $x_{cg} - (C_{m\alpha} / C_{N\alpha})$
α	=	angle of attack, deg
ε	=	turbulence dissipation rate, m^2/s^3
ρ	=	density, kg/m^3

*Aerospace Engineer, Weapons & Materials Research Directorate, AMSRD-ARL-WM-BC, Associate Fellow.
†Mathematician, Weapons & Materials Research Directorate, AMSRD-ARL-WM-BC, non-member.

I. Introduction

The use of computational fluid dynamic (CFD) calculations to accurately predict the aerodynamic coefficients and flow phenomena of many geometrically complex, single-body and multi-body systems has been previously demonstrated using commercial and Government sponsored CFD software packages.[1–7] However, it is yet to be demonstrated that CFD can accurately predict the Magnus moment and roll damping moment of relatively simply shaped, spin-stabilized projectiles across the full Mach number range, from subsonic to supersonic. A recent study[8] demonstrated limited success in predicting the Magnus moment of a 12.7-mm (0.50 caliber) projectile. The prediction of Magnus moment in the subsonic and supersonic regimes was found to be fair, but in the transonic regime it was not as good. The effect of not modeling the engraving on the body of the projectile was not determined. Earlier numerical studies investigating spin-stabilized projectiles[9–11] were limited in scope, primarily because of limited computational resources. A thorough study should investigate the full Mach number range, from subsonic through supersonic, as in Ref. 8 and the present study.

The projectile chosen for this study was the M910 target practice, discarding sabot-traced (TPDS-T) projectile.[12] The M910 was developed by the U.S. Army as an aeroballistic match to the M791 armor-piercing, discarding sabot-traced (APDS-T) service ammunition fired from the 25-mm M242 chain gun mounted on the Bradley Fighting Vehicle. The M910 sub-caliber projectile is illustrated in Fig. 1. The requirements for an aeroballistic match usually are:

- limitation on the time of flight (TOF) difference between the training and service munitions at the service munition effective range,
- limitation on the center of impact difference (e.g. 1 milliradian) between the training and service munitions over the entire range,
- limitation of the maximum range of the training projectile (e.g. 8000 m), which includes the ricochet safety danger zone, and
- the training projectile will have a dispersion that does not exceed the dispersion of the service ammunition by more than 10%.

In order to design a projectile that is an aeroballistic match to a service ammunition, the aerodynamic coefficients must be predicted to within engineering accuracy. The aerodynamic coefficients are usually initially determined by using semi-empirical engineering codes, or they are determined experimentally in an aeroballistic range or wind tunnel. During the design phase, an engineering code is usually used to develop candidate designs that are then fired in the aeroballistic range to confirm the aerodynamics. Table 1, which is excerpted from Ref. 13, presents estimated errors expected in data obtained from three sources. The data indicate that, in general, the aeroballistic range provides more accurate aerodynamics than either the wind tunnel or engineering codes.

It would be beneficial if CFD could sometimes be used in place of the aeroballistic range to confirm the aeroballistics of a candidate design. It must be demonstrated that CFD can not only accurately predict the aerodynamic coefficients, especially the Magnus moment, but also show that the complete study can be done with reasonable computational resources in a reasonable time frame. Performing an experimental investigation in an aeroballistic range can take a minimum of weeks, including design and fabrication of the projectiles, scheduling of the experimental facility, and data reduction. A CFD investigation should be feasible in a similar time frame, once it is determined what simulation conditions, such as mesh characteristics, turbulence model, etc., provide accurate

Table 1. Expected Aerodynamic Coefficient Percent Errors.[13]

Aerodynamic Coefficient	Wind Tunnel	Aeroballistic Range	Spinner-98 (PRODAS)
Axial Force	5–10	0–2	3–5
Normal Force	3–7	4–8	6–10
Magnus Force	Large	25	33
Pitching Moment	5–10	0–3	3–6
Pitch Damping Moment	Large	10–20	15–25
Magnus Moment	Large	10–20	15–25
Roll Damping	Large	5–10	10–15

predictions. This assumes that mesh generation will not take an inordinate amount of time, which is reasonable, since spin-stabilized projectiles usually provide some of the less demanding models to mesh. This study is an attempt to determine the feasibility of CFD to provide accurate and timely predictions of spin-stabilized projectile aerodynamic coefficients. Specifically, the conditions necessary for the accurate calculation of the Magnus and roll damping moments are investigated. The pitch damping coefficient is not addressed in this study, but recent work has addressed calculating the dynamic stability derivatives using CFD.[14–16]

II. Numerical Approach

A. Computational Geometry and Mesh

The computational model of the M910 sub-projectile is shown in Fig. 1. The aluminum nose consists of a 0.22-cm meplat, followed by a 4.12-cm conical ogive. The ogive is followed by a 1.62-cm diameter (1-caliber) cylindrical, steel body, 3.27 cm long. A 0.2-cm chamfer forms the base of the projectile. The center of gravity is located 4.99 cm from the nose. All moments in later sections are referenced from the center of gravity.

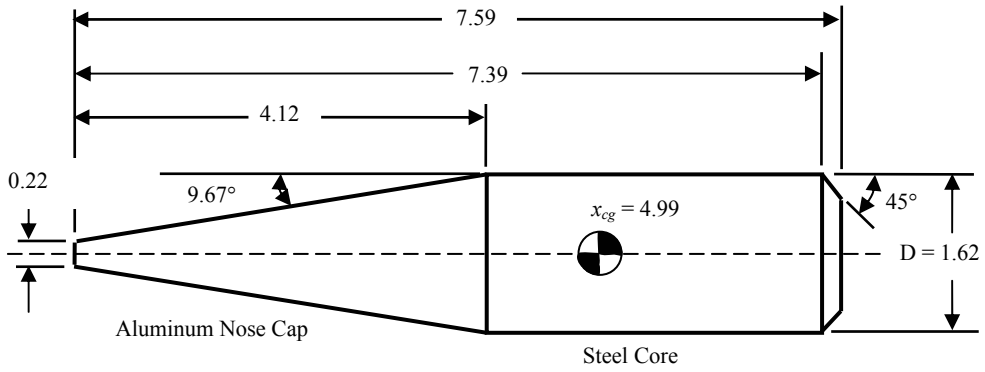

Figure 1. Schematic of the 25-mm M910 TPDS-T Projectile.

The geometry and unstructured mesh were generated using GAMBIT, a geometry and grid preprocessor supplied with the FLUENT CFD software suite.[17] A full three-dimensional (3-D) mesh was required to simulate the spinning shell at angle of attack. In generating the meshes, boundary layer (B.L.) mesh spacing was used near the projectile body. The last column of Table 2 lists the first-edge spacing used for each mesh. The y^+ value is actually based on the first cell centroid, or one-half of the first-edge spacing. Resolving the viscous boundary layer is critical for predicting the Magnus and roll damping moments; therefore, wall functions were not used and the option to integrate the equations to the wall was used. Normally, a y^+ value on the order of 1.0 is adequate to resolve the boundary layer. However, it was desired to have a y^+ value of 0.5 or less to ensure capturing the Magnus effect of the spinning shell. All mesh stretching ratios were kept to 1.25 or less.

Two meshes were originally generated; one for supersonic calculations ($M > 1.4$), and one for subsonic and transonic calculations ($M \leq 1.4$). These are listed as Mesh 1 and Mesh 2, respectively, in Table 2. A 31% savings in mesh size was achieved by using the more compact supersonic mesh when possible. However, initial calculations showed that the Magnus and roll damping moments were not accurately calculated in the subsonic and transonic flow cases. Also, the y^+ value at the projectile surface was above 0.5 for the supersonic flow cases. The supersonic mesh was then modified, decreasing the boundary layer first-edge spacing, and increasing the mesh density in the projectile wake flow region. The subsonic/transonic mesh was also

Table 2. Computational Mesh Characteristics.

Case	Number Cells	Radial Boundary (cal.)	Front Boundary (cal.)	Rear Boundary (cal.)	First B.L. edge (cal.)
Mesh 1	1,139,056	3.51	0.31	5.31	4.00×10^{-5}
Mesh 2	1,651,680	45.8	24.7	39.8	4.00×10^{-5}
Mesh 3	1,952,480	3.51	0.31	5.31	1.54×10^{-5}
Mesh 4	1,960,928	45.8	24.7	39.8	4.00×10^{-5}

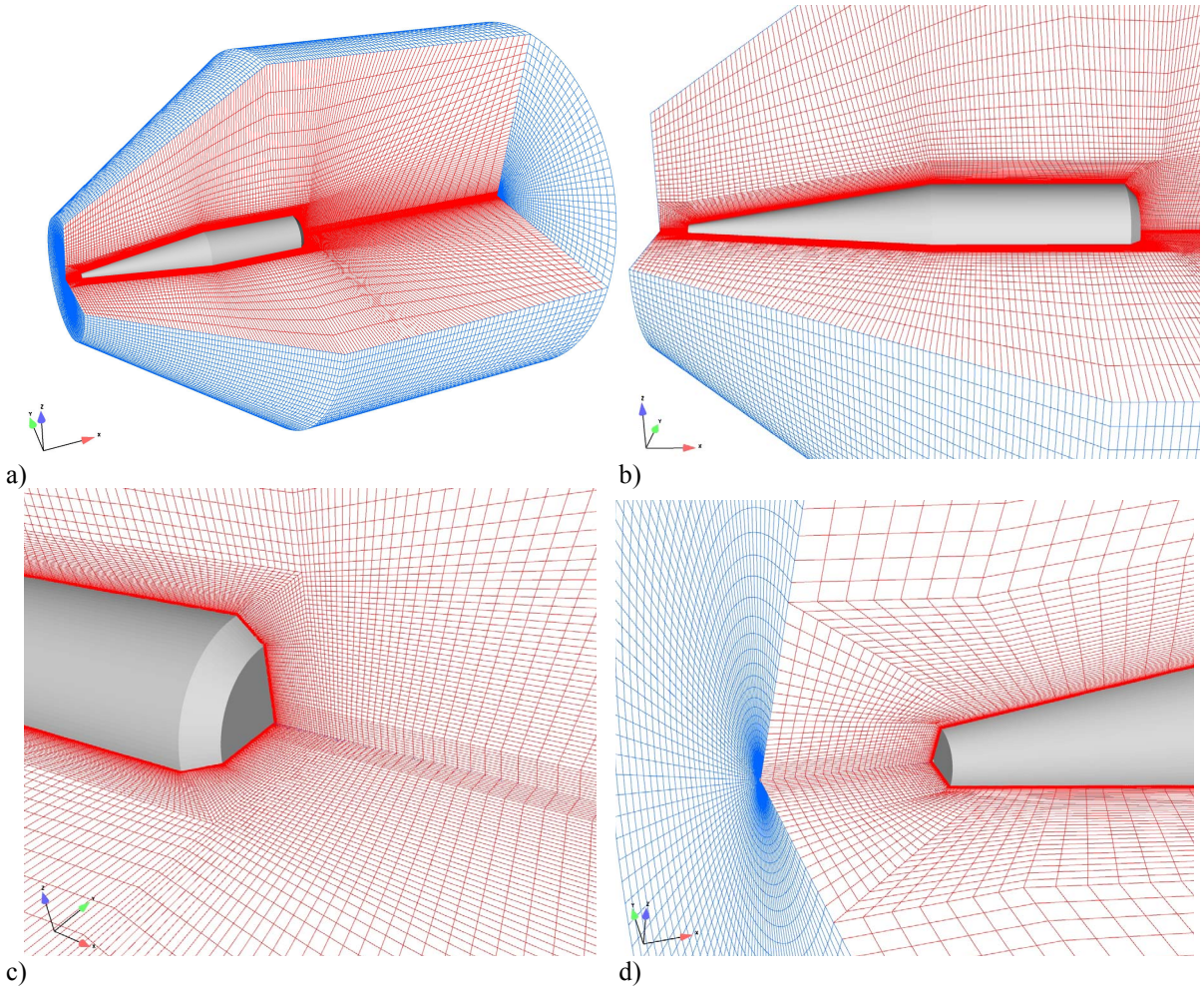

Figure 2. Computational mesh for supersonic cases (M > 1.4); (a) full domain, (b) side view showing O-grid near projectile, (c) base region, and (d) nose region.

modified, increasing the mesh density in the wake flow region. The characteristics of the new meshes are listed in Table 2 as Mesh 3 and Mesh 4, respectively. The size of the supersonic mesh increased dramatically due to the smaller boundary layer first-edge spacing. The size of the two new meshes increased to 1.9 M cells, but the benefit of using the supersonic mesh is still realized.

The meshes consist almost entirely of hexahedral cells; the only exceptions are some wedge shaped prisms in front of the nose, along the axis of the projectile. Figures 2 and 3 show views of the computational meshes used for the supersonic cases (Mesh 3) and subsonic/transonic cases (Mesh 4), respectively. The properties of the two meshes are compared in Table 2, including the location of the outer boundary of the computational domain with respect to the projectile. The near body region of both meshes was similar, with Mesh 4 generated by making another mesh around Mesh 3 (e.g., see Fig. 3b). An O-grid was manually generated around the projectile body, building a boundary layer mesh off the entire projectile surface. The circumferential direction contained 136 cells. The mesh density in Mesh 3 and Mesh 4 was increased in the wake region by reducing the axial stretching ratio to 1.05–1.10.

The boundary conditions were as follows. The outer boundaries were set as far-field (characteristics-based inflow/outflow), with standard temperature and pressure free-stream conditions (101.325 kPa, 288 K). The projectile wall was modeled as a no-slip, isothermal (288 K) wall boundary, rotating around the x-axis at the specified spin rate. Table 3 shows the conditions used for initializing the flow field at the specific Mach numbers investigated in the study. The projectile spin rates were determined from the muzzle exit twist of the M242 gun, which is 23.9 calibers per revolution.

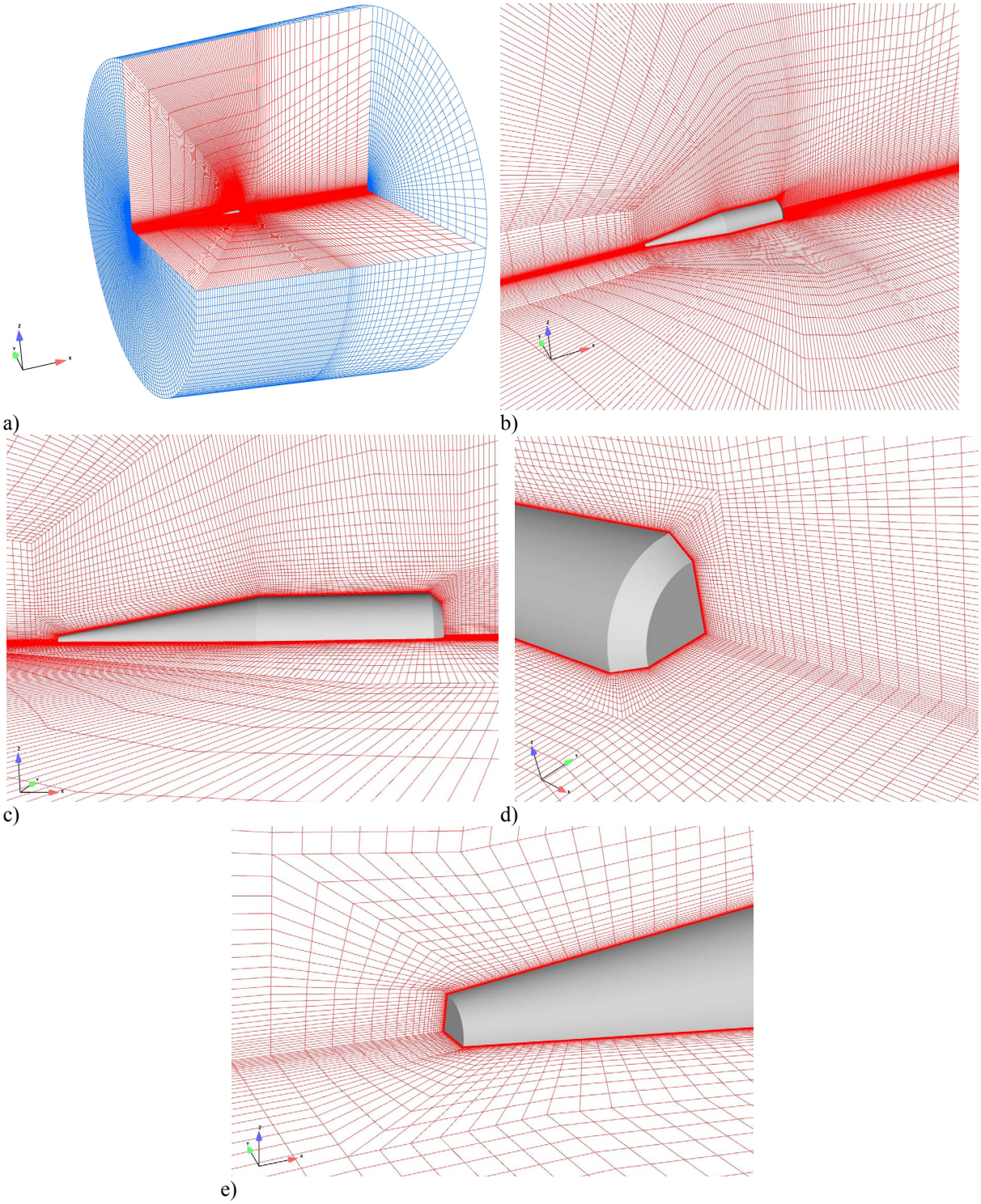

Figure 3. Computational mesh for subsonic and transonic cases ($M \leq 1.4$); (a) full domain, (b) near-body region (c) side view showing O-grid around projectile, (d) base region, and (e) nose region.

A grid resolution study was conducted for the Mach 2.5 case. For this study, Mesh 1 was both coarsened (642,180 cells) and refined (2,217,888 cells) in all three directions. The first-edge spacing (4×10^{-5} cal.) was kept constant in all three meshes, but the number of cells near the body was changed via different stretching ratios.

Table 3. Flow Conditions and Spin Rate vs. Mach Number.

Mach Number	U_∞ (m/s)	Reynolds Number (m^{-1})	Total Pressure (kPa)	Total Temperature (K)	Spin rate (rad/s)
0.40	136.1	9.32×10^6	113.1	297.2	1431
0.50	170.1	1.17×10^7	120.2	302.4	1789
0.60	204.1	1.40×10^7	129.2	308.7	2147
0.70	238.1	1.63×10^7	140.5	316.2	2504
0.90	306.2	2.10×10^7	171.4	334.7	3220
0.98	333.4	2.28×10^7	187.4	343.3	3506
1.02	347.0	2.38×10^7	196.4	347.9	3649
1.20	408.2	2.80×10^7	245.7	370.9	4292
1.40	476.3	3.26×10^7	322.4	400.9	5009
2.00	680.4	4.66×10^7	792.8	518.4	7153
2.50	850.5	5.83×10^7	1731.2	648.0	8944
3.50	1190.7	8.16×10^7	7728.3	993.6	12522
4.50	1530.9	1.05×10^8	29324.9	1454.4	16100

B. Navier-Stokes CFD

The commercially available CFD^{++} code,[18] version 3.5.1, was used in this study. The CFD^{++} code can simulate a range of fluid dynamic phenomena, ranging from incompressible to hypersonic flow. The 3-D, time-dependent, Reynolds-averaged Navier-Stokes (RANS) equations are solved using the finite volume method. The implicit solver with dual time-stepping was used. The spatial discretization was a second-order, multi-dimensional Total Variation Diminishing (TVD) polynomial interpolation scheme. Solutions to semi-infinite "Riemann problems" are used in CFD^{++} to provide upwind flux information to the underlying transport scheme. Approximate Riemann solvers are used to determine the higher order fluxes to avoid spurious oscillations that may become physically unbounded if determined via fixed-stencil interpolation. The preconditioned form of the governing equations was used for $M \leq 1.4$. Preconditioning the equations ideally equalizes the eigenvalues of the inviscid flux Jacobians and removes the stiffness arising from large discrepancies between the flow and sound velocities at low speeds. Although usually needed for low Mach number ($M \leq 0.2$) flows, preconditioning was found to improve the convergence characteristics through the transonic flow regime, likely due to the low speed flow in the projectile wake region. Far-field absorbing layers were also used on the outer boundaries for $M \leq 1.4$, improving convergence and reducing oscillations in the equation residuals and force/moment iteration histories.

Several turbulence modeling approaches were investigated. The two-equation, "realizable" k-ε turbulence model, which solves transport equations for the turbulence kinetic energy, k, and its dissipation rate, ε, is the recommended general use model and was initially used in this study. The realizable variant accounts for certain known physical properties of the stress tensor by introducing a bound on the magnitude of the predicted tensor components, improving the predictive accuracy and stability.[18] When initial calculations did not accurately predict the Magnus and roll damping moments in the subsonic and transonic flow regimes, and the aforementioned mesh modifications did not improve the results, several other available turbulence models were investigated. These include the one-equation R model, which solves directly for the undamped eddy viscosity, R; and the three-equation k-ε-R model, which solves turbulence transport equations for k, ε, and R. CFD^{++} also has available Large-Eddy Simulation (LES) models and a hybrid RANS/LES detached-eddy simulation (DES) model (termed LNS in CFD^{++}). The time-accurate DES calculation takes substantially more computation time than the steady state calculations, compromising one of the goals of the investigation.

Table 4. Percent differences from medium mesh in grid resolution study at $M = 2.5$.

Mesh	α (°)	C_D (%)	$C_{L\alpha}$ (%)	$C_{m\alpha}$ (%)	C_{lp} (%)	$C_{Yp\alpha}$ (%)	$C_{np\alpha}$ (%)
Coarse	2	0.06	-0.55	-0.69	-1.29	0.75	-1.26
	3	0.22	-0.48	-0.56	-1.09	1.87	2.82
	5	0.35	-0.26	-0.44	-0.52	-0.89	10.93
fine	2	-0.85	-0.32	-0.23	-1.49	2.33	8.78
	3	-0.73	-0.32	-0.18	-1.40	1.90	-2.87
	5	-0.55	-0.29	0.10	-1.21	0.50	-0.09

The simulations were performed in parallel on an IBM SMP P3 with Power3 processors. To achieve optimum parallel performance, the solutions were run with about 120,000–140,000 cells on each processor (e.g., 8 processors for Mesh 1, 12 processors for Mesh 2, and 16 processors for Mesh 3 and Mesh 4). The calculations took about 25–40 s of CPU time per iteration (wall-clock time was similar) and convergence was achieved in about 500–2500 iterations, depending on the Mach number and turbulence model. The solution was deemed converged when the flow residuals had reduced at least 3 orders of magnitude and the aerodynamic coefficients changed less than about 0.5% over the last 100 iterations. The aerodynamic coefficients were the determining factor in convergence in all cases The investigations using the realizable k-ε and R turbulence models each consisted of 39 cases–13 Mach numbers and three angles of attack ($\alpha = 0°$, 3°, and 5°). The investigation using the k-ε-R model was only performed at $\alpha = 3°$, but over the entire Mach number range. The DES calculation was only performed at $\alpha = 3°$ and 7 Mach numbers, $M = 0.4$, 0.6, 0.9, 1.02, 1.4, 2.5, and 4.5. The time steps used in the DES calculations ranged from a maximum of 5.0×10^{-6} at $M = 0.4$ down to 1.0×10^{-6} at $M = 4.5$. These values were based on the period of the oscillations in the wake flow, assuming a Strouhal number of 0.25. Five inner iterations were performed at each time step. The final solution of a steady-state solution was used as the initial conditions for the time-accurate DES calculations.

The single precision solver was used, and several checks with the double precision solver showed no significant difference in the calculated results. The maximum Courant-Friedrich-Lewy (CFL) number was chosen using the recommendations within the CFD^{++} solver:

- subsonic ($0.3 < M < 0.7$), CFL ramped from 1.0 to 100.0 over 100 iterations,
- transonic ($0.7 < M < 1.4$), CFL ramped from 1.0 to 75.0 over 100 iterations,
- low supersonic ($1.4 < M < 2.0$), CFL ramped from 1.0 to 30.0 over 100 iterations,
- mid supersonic ($2.0 < M < 4.0$), CFL ramped from 1.0 to 40.0 over 100 iterations, and
- hypersonic ($M > 4.0$), CFL ramped from 0.1 to 20.0 over 200 iterations.

C. Semi-Empirical Method

Solutions were also obtained with the semi-empirical, engineering design code PRODAS, which is an acronym for Projectile Design / Analysis System.[13] This code provides solutions in seconds and is used to quickly determine aerodynamic coefficients, stability characteristics, trajectories, and other information for the projectile designer. The development of PRODAS originated at General Electric in 1972 and has continued at Arrow Tech Associates, Inc., since 1991. PRODAS was developed using proven methodologies and techniques such that performance predictions are based in part on prior experimental testing.

III. Results and Discussion

A. Grid Resolution Study

A grid resolution study was conducted for the Mach 2.5 case at $\alpha = 0°$, 2°, 3°, and 5°. The solutions on the coarse (0.6 M cell), medium (1.1 M cell), and fine (2.2 M cell) meshes were compared for differences in the aerodynamic coefficients. Table 4 shows the results of the study, specifically the percent difference between the

indicated mesh and the medium mesh. The $\alpha = 0°$ case is not included because all but the drag and roll damping coefficients are near zero.

The differences in drag, lift, and pitching moment coefficients due to mesh size were less than 1%. The difference in roll damping coefficient was less than 1.5%. The Magnus force and moment coefficients showed larger changes. The Magnus force and moment coefficients are relatively small coefficients, especially at low α, and are the hardest to predict accurately. The maximum difference was less than 3% for the Magnus force coefficient and less than 11% for the Magnus moment coefficient. The fine mesh solution improves the Magnus moment coefficient values by 9% at $\alpha = 2°$, but the improvement is less than 3% at higher α.

This study indicates that even the coarse mesh may be adequate if the lift, drag, pitching moment, and maybe even the roll damping moment were desired. However, even the modest improvement in the Magnus force and moment provided by the medium mesh makes it more suitable because of the importance in predicting these values. It is not deemed worth the added computational resources to use the fine mesh to gain less than 3% improvement in Magnus moment coefficient at $\alpha > 2°$. In the main study, the force and moment derivatives are all based on $\alpha = 3°$.

We note that the reason the coarse mesh provides fairly reasonable results is that the medium mesh was designed based on our past experiences and knowledge of what type of mesh is required to accurately predict the aerodynamic coefficients for non-spinning projectiles and missiles. This generally leads to meshes that provide highly resolved flow features. Generating the coarse mesh by halving the dimensions of the medium mesh still left a relatively good mesh. One purpose of the current investigation is to determine the proper mesh characteristics required to accurately predict the aerodynamic coefficients (specifically, Magnus moment) of spinning projectiles.

The grid resolution study was performed using the realizable k-ε model on meshes based on Mesh 1. Although a specific grid resolution study was not performed at other Mach numbers, the results of subsequently moving to Mesh 3 and Mesh 4 showed that the increased mesh density in the wake and lower y^+ values (Mesh 3, with resulting increased mesh density near projectile body) did not result in noticeable changes in the aerodynamic coefficients. As will be shown below, the choice of turbulence model has the largest effect on the aerodynamic coefficients, primarily the Magnus moment and roll damping.

B. Comparisons of CFD with Experimental Data and PRODAS

The experimental data from Reference 12 is used here to validate the CFD results. The values of expected percent error in the aerodynamic coefficients obtained from the aeroballistic range and PRODAS predictions (Table 1) should be considered when viewing the results, especially the experimental data for Magnus moment and roll damping.

Figure 4 shows the zero-yaw drag coefficient as a function of Mach number, comparing the CFD^{++} predictions to both the experiment and the PRODAS prediction. Results are only shown for the realizable k-ε (rke) and R (Rt) turbulence models, as the other turbulence model cases were not run at $\alpha = 0°$. PRODAS predicts C_{D0} well for $M \geq 0.9$. Both CFD^{++} cases are within 10% of the experimental data over the Mach number range. CFD^{++} predicts the drag slightly higher than PRODAS and the experiment for $M \geq 1.0$. The one-equation R turbulence model actually provides a better prediction than the realizable k-ε model for $M < 0.9$, a difference of about 10% at $M = 0.4$. The realizable k-ε model provides a slightly better prediction than the R model in the range $1.0 < M < 2.0$. The two models provide nearly the same results for $M \geq 2.0$.

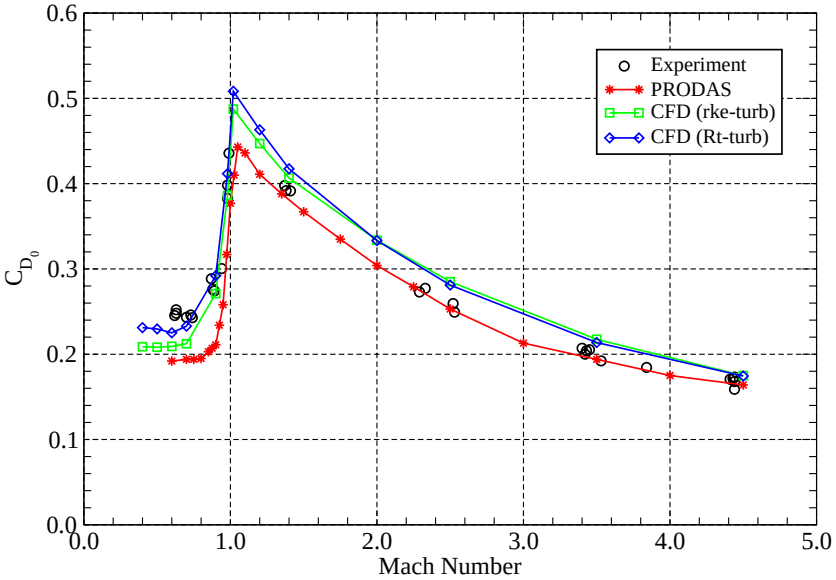

Figure 4. Zero-yaw drag coefficient vs. Mach number.

Figure 5 shows the comparison of the drag coefficient at $\alpha = 3°$. Results are now included for the k-ε-R and DES turbulence models. Note again that only 7 Mach numbers were investigated in the DES cases. All the CFD^{++} cases accurately predict C_D at this angle of attack over the entire Mach number range. The PRODAS predictions are a little low for $M > 2.5$, while the CFD^{++} are slightly high for $M < 2.5$. The realizable k-ε model predictions are again a little low for $M < 0.9$ and for $1.0 < M < 1.4$. The three equation k-ε–R model provides a drag prediction similar to the R model over the Mach number range. The DES predictions are very close to the steady-state CFD^{++} cases. This result demonstrates that steady state calculations can accurately predict the drag, since the DES calculations can be considered the most accurate of the group.

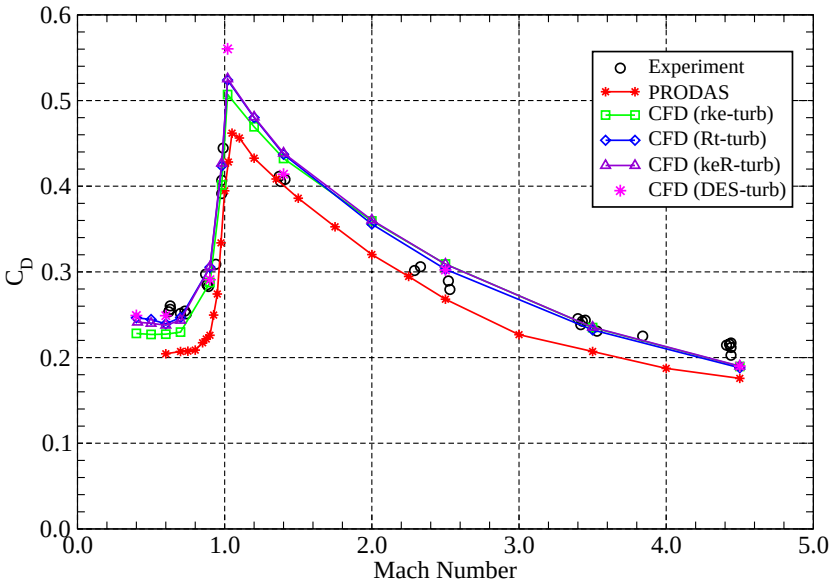

Figure 5. Drag coefficient at 3° yaw vs. Mach number.

The normal force coefficient as a function of Mach number is shown in Fig. 6. PRODAS and all the CFD^{++} cases predict $C_{N\alpha}$ well over the Mach number range. The predictions are higher than the experimental data in the supersonic flow regime, but are still within 10% of the mean. CFD^{++} predicts the increase in normal force at $M = 1.0$, which PRODAS does not. A peak in the lift coefficient at $M = 1.0$ was also evident in the data fits plotted in Ref. 12, which are not reproduced here. The two subsonic DES cases predict normal force coefficients that are too high, which is puzzling. However, it is interesting to note that one experimental data point near $M = 0.6$ is nearly equal to the DES prediction at that Mach number. These two subsonic cases will be run for longer times to see if the normal force decreases to values nearer the steady state and experimental mean values. The results from the three steady state turbulence model predictions are nearly indistinguishable. In the transonic and supersonic flow regimes, the DES calculations are again very close to the steady state cases, demonstrating the adequacy of the latter to predict the normal force.

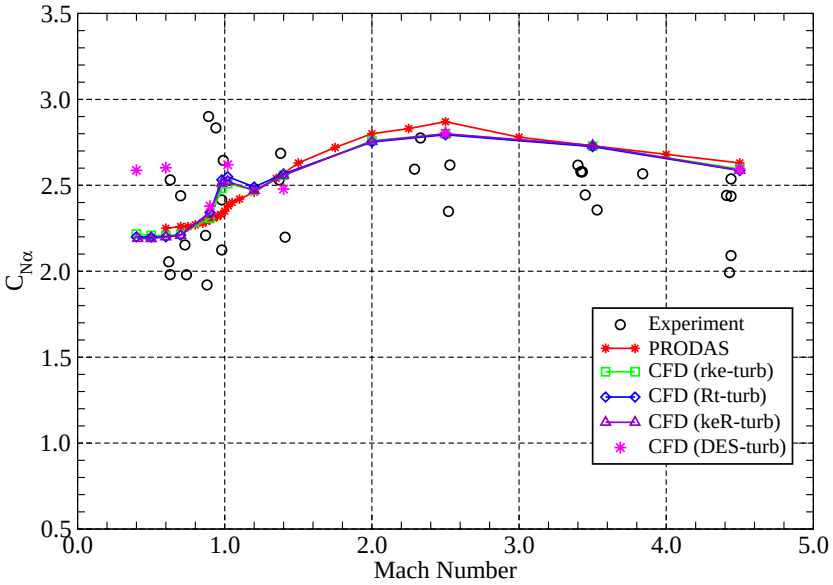

Figure 6. Normal force coefficient derivative vs. Mach number.

The pitching moment coefficient as a function of Mach number is shown in Fig. 7. The CFD^{++} cases predict $C_{m\alpha}$ very well over the entire Mach number range. The PRODAS predictions are a little high for $M > 2.5$, and a little low in the transonic flow regime. The steady-state CFD^{++} cases catch the small increase in $C_{m\alpha}$ at $M = 0.98$, while the DES calculations were not run at this Mach number. The two subsonic DES cases are too low, which follows from the high prediction of $C_{N\alpha}$. Again, the results from the three steady state turbulence models are nearly

indistinguishable and the DES calculations are very close to the steady state cases in the transonic and supersonic flow regimes.

The normal force center of pressure as a function of Mach number is shown in Fig. 8. The calculated results compare very well, following the trends in the normal force and pitching moment coefficients, from which x_{cp} is calculated. All four turbulence models compare very well, with the noted exception of the two subsonic DES calculations.

The quality of the CFD^{++} predictions for the coefficients shown so far is not surprising, since previous investigations have demonstrated the capability of CFD to predict these aerodynamic coefficients. However, in the present study, the roll damping and Magnus moment coefficients are the parameters of interest. Figure 9 shows the roll damping coefficient as a function of Mach number. The CFD^{++} values were calculated at $\alpha = 3°$, but the roll moment was found to be independent of α for the range investigated. A cubic fit of the experimental data is also shown in the figure to visualize the trend. Note that the expected error in the aeroballistic range data is 5–10% (Table 3). The PRODAS and realizable k-ε model CFD^{++} predictions are nearly identical for $M < 1.8$. The PRODAS predictions are too low above $M > 2.5$, while all the CFD^{++} calculations predict C_{lp} fairly well for $M \geq 2.0$. The PRODAS and the CFD^{++} predictions are within the upper bound of the maximum expected error in the experimental data for $0.9 < M < 2.0$. However, in general, PRODAS and the realizable k-ε model CFD^{++} predictions do not accurately capture the downward trend in the experimental data shown by the cubit fit, a difference of about 20% at $M = 0.6$. The three-equation k-ε-R turbulence model improves the prediction of C_{lp} in this Mach number range, resulting in a difference of less than 15% at $M = 0.6$. The calculations with the one-equation R turbulence model provide the closest prediction to the experimental data for $M < 2.0$. The DES calculation results, which are expected to be the most accurate, are very close to the k-ε-R turbulence model results for $M \leq 1.4$. Both these calculations fall near the upper bound of the maximum expected error in the experimental data. The k-ε-R turbulence model is recommended for the calculation of C_{lp}, since it compares well with the DES calculations over the entire Mach number range. Although it is usually desired to predict the aerodynamic coefficients to within at least 10% of the experimental data, these results demonstrate that steady state calculations are adequate for the prediction of the roll damping

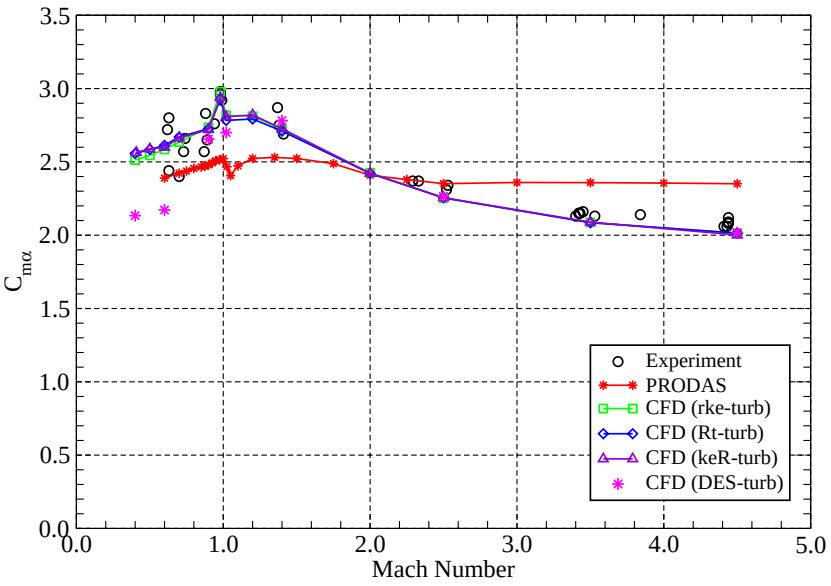

Figure 7. Pitching moment coefficient derivative vs. Mach number.

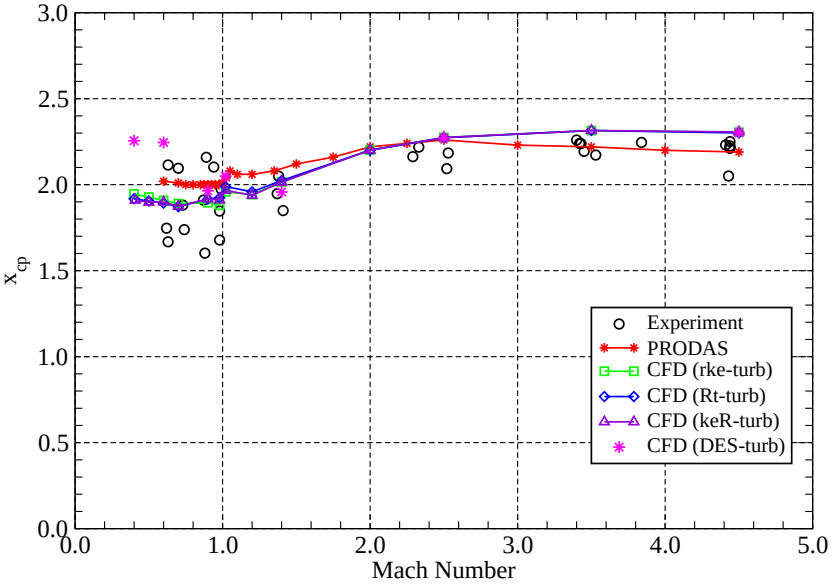

Figure 8. Normal force center of pressure location vs. Mach number.

coefficient, considering the small absolute values involved. However, as usual, care must be taken to choose the appropriate turbulence model.

The Magnus moment coefficient at $\alpha = 3°$ as a function of Mach number is shown in Fig. 10. The zero-yaw Magnus moment and cubic Magnus moment coefficients from Ref. 12 were used to transform the experimental data to obtain $C_{np\alpha}$ at $\alpha = 3°$. A cubic fit of the experimental data is again shown in the figure to visualize the trend. Note that the expected error in the aeroballistic range data is 10–20% (Table 3). None of the steady-state CFD^{++} calculations, nor PRODAS, predict the decreasing trend of $C_{np\alpha}$ below $M = 2.0$. The inadequacy of the steady-state CFD cases to predict the Magnus moment was the impetus to investigate using a time-accurate calculation. Rather than use unsteady RANS calculations, we took advantage of the hybrid RANS/LES, or detached eddy simulation, capability in CFD^{++}. As seen in Fig. 10, the DES calculations more accurately predict the Magnus moment in the subsonic and transonic flow regimes. There is a drastic increased cost in computational time required, which is discussed later. For $M < 1.4$, the error in the DES data points may be as high as in the experimental data, due to the large amplitude, oscillatory nature of the force and moment time histories. For cases below $M = 1.4$, the oscillations in the force and moment time histories made it difficult to determine the mean value. This is illustrated in Fig. 11, which shows the Magnus moment coefficient vs. time for three Mach numbers, one in each flow regime, from the DES calculations, which were run for between 2–4 projectile spin cycles. The magnitude of the oscillations decreases with increasing Mach number. These oscillations appear to be a result of the influence of the oscillatory wake flow, which is illustrated in the next section. The predictions in the supersonic range, above $M = 2.5$, are also not as accurate as desired. The DES predictions are actually negative over the entire Mach number range, even above $M = 2.0$, where the experimental data and the other predictions are positive.

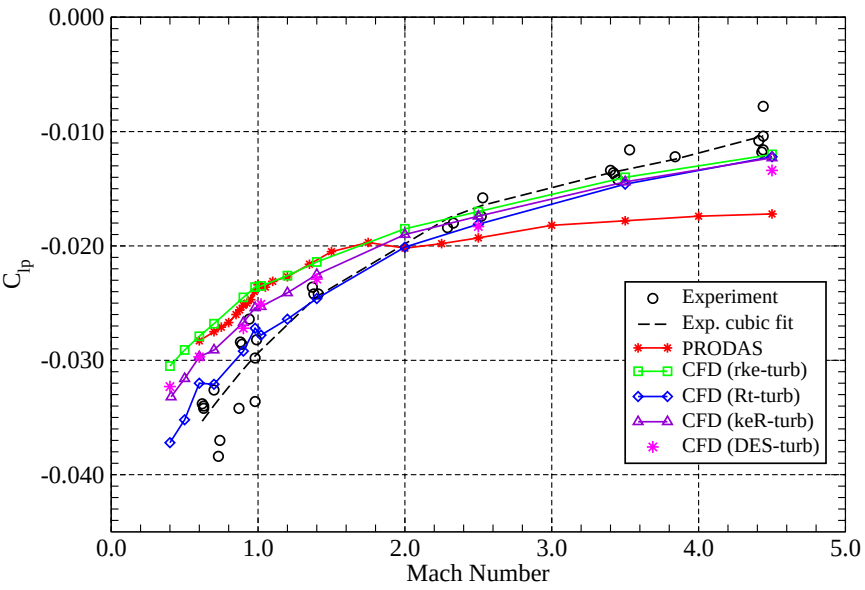

Figure 9. Roll damping coefficient vs. Mach number.

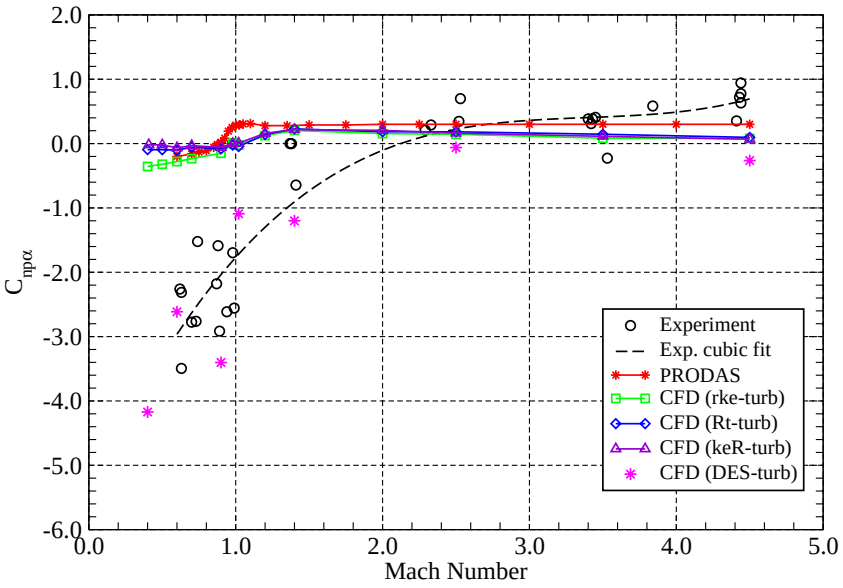

Figure 10. Magnus moment coefficient derivative vs. Mach number at $\alpha = 3°$.

Above $M = 2.0$, the experimental values and CFD^{++} predictions of $C_{np\alpha}$ are near zero, indicating that the Magnus force center of pressure is very near the center of gravity, x_{cg}. The measurement of Magnus moment in the aeroballistic range is difficult, and having the Magnus force center of pressure so near the moment reference point may lead to additional uncertainty. It will be advantageous to re-analyze the experimental data using modern data reduction tools to determine if the quality of the experimental data can be improved. The comparison between CFD

and the experimental data was improved in the investigation reported in Ref. 8, after re-reducing the data with modern data reduction software. This data reduction procedure is planned, but was not able to be performed in time to include in this paper.

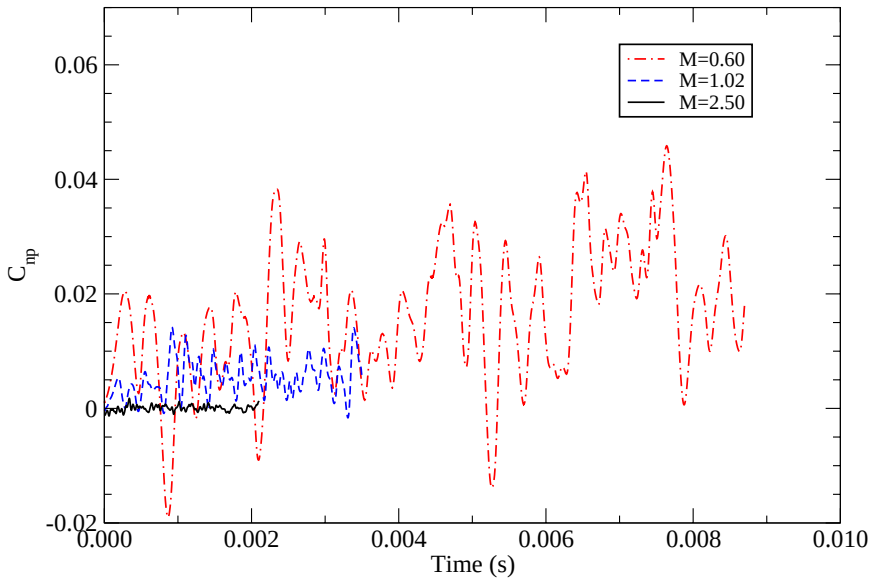

Figure 11. Magnus moment coefficient vs. time for $\alpha = 3°$.

C. Discussion

The steady state calculations are adequate to predict all the aerodynamic coefficients except the Magnus moment. The results are deemed mesh independent from the study described in Section III A, and also from the observation that the increase in mesh quality using Mesh 3 and Mesh 4 did not significantly change any of the calculated aerodynamic coefficients. The y^+ values in the mesh boundary layer were adequate. Figure 12 shows the calculated y^+ values on the leeward side of the projectile at $\alpha = 3°$. The y^+ values for the subsonic and transonic cases (Fig. 12a) are all less than 0.5. Three supersonic cases (Fig. 12b) have y^+ values less than 0.5. The $M = 4.5$ case is greater than 0.5 on about one-half of the ogive length, but the y^+ is still less than about 0.65.

The dramatic difference in the accuracy of the Magnus moment prediction via the time-accurate DES calculation vs. the steady state calculations in the subsonic and transonic regimes indicates that the oscillatory wake flow impacts the upstream side forces. The effect is most dramatic in the subsonic and transonic flow regimes. Comparing the viscous and inviscid components of the Magnus moment, it was observed that the viscous component was about 40–60% of the total moment in the steady state cases (k-ε-R model), while it was less than 10% in the DES cases for $M \leq 1.0$. Above $M = 1.0$, the viscous component was less than 10% of the total moment for both the steady state and time accurate calculations. Still, the inviscid (pressure) component of the moment followed the same overall trends as the total moment.

An observation of differences in the flow fields calculated by the steady state vs. the time-accurate DES helps explain the phenomena. Figures 13–17 show Mach contours on the pitch plane at the indicated Mach numbers for the steady-state k-ε-R and time-accurate DES calculations. At all Mach numbers, both calculations show similar flow structures over the projectile forebody. The flow remains subsonic over the entire field in the $M = 0.6$ case (Fig. 13). In the $M = 1.02$ case (Fig. 14), expansion fans and recompression shocks aft of the ogive-body interface and projectile base are observed. At $M = 1.4$ and above (Fig. 15–17), a well defined oblique shock has formed at the nose, and the expansion and recompression shock waves farther aft have become more well defined.

The differences in the steady state vs. time accurate results are most noticeable in the projectile wake flow. At $M = 0.6$ and 1.02, there is a flow pattern similar to vortex shedding past a bluff body. At the higher Mach numbers, the differences are primarily the increased structure in the base flow region in the DES cases, since this is lost in the averaging in the steady-state RANS calculations.

More detailed analysis of the local forces on the projectile will be necessary to fully quantify the flow field and Magnus observations in the DES calculations. The effects on the body forces are small enough not to significantly affect the normal forces. However, the Magnus force is much smaller and is obviously affected by the transient flow in the projectile wake, at least in the subsonic and transonic flow regimes.

Another goal of the study was to demonstrate that the CFD calculations could be performed in a "reasonable" time frame. Table 5 lists the estimated average time required to calculate one case (one Mach number, one angle of attack) for the four turbulence models investigated. The three steady state cases have comparable calculation times. The three-equation k-ε-R model provided very good convergence properties, thereby resulting in lower total computational time than the two-equation k-ε and one-equation R model cases. Using the k-ε-R model case as an example, a study consisting of 13 Mach numbers and 3 angles of attack would take approximately 11 days to

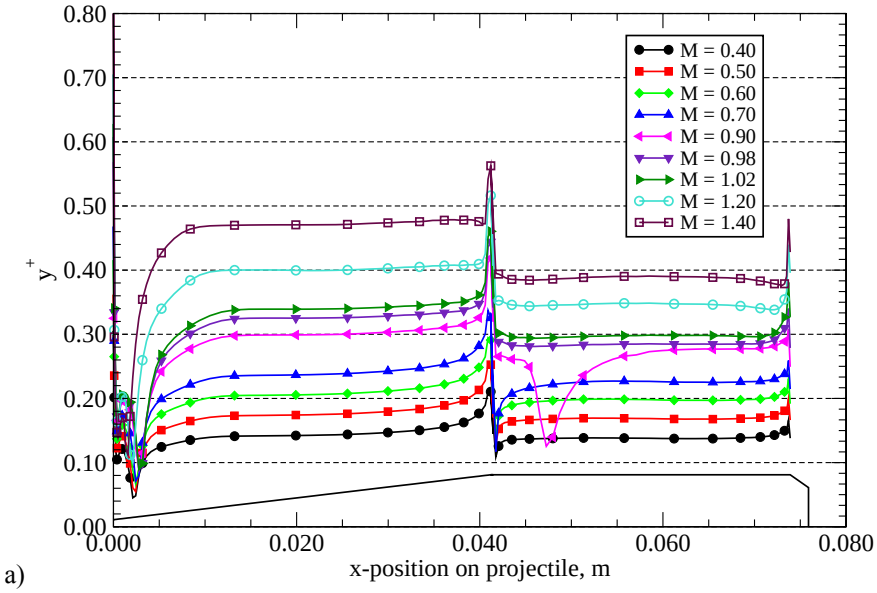

a)

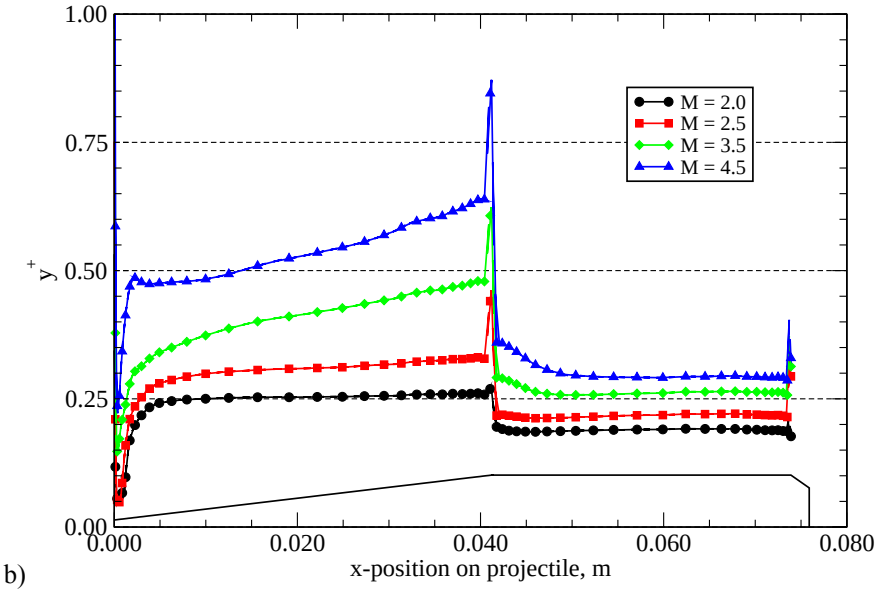

b)

Figure 12. Post-run calculated y^+ values on leeward side of projectile, $\alpha = 3°$; (a) subsonic and transonic cases and (b) supersonic cases.

complete on the IBM SP3 used in this study. However, this assumes that the cases are run sequentially. Several cases were actually run concurrently, and a complete study of 39 cases was completed in less than one week. As

Table 5. Estimated CPU/wall clock time required per case.

Turbulence Model	No. iterations/time steps required	Time per iteration/time step (s)	Total time Required (hr)
Realizable k-ε	950	35	9.2
R	700	35	6.8
k-ε-R	725	35	7.0
DES	1500	200	83.3

Table 5 indicates, the time to complete the time-accurate DES calculation is about 10 times that of the steady state cases. However, the time-accurate DES calculation is only required for the Magnus moment calculation for $M < 2.0$. Therefore, a smaller number of time-accurate cases may be required at several Mach numbers, and only one or two angles of attack, in order to determine the variation of Magnus moment with Mach number.

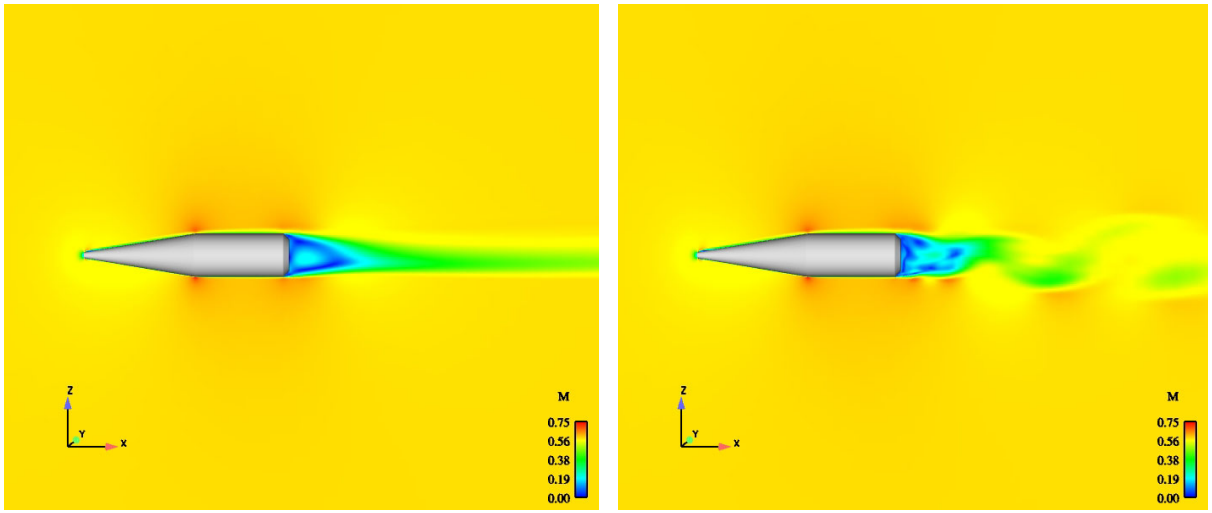

a) b)

Figure 13. Mach number contours on pitch plane at $M = 0.6$; (a) steady state k-ε-R and (b) time-accurate DES model.

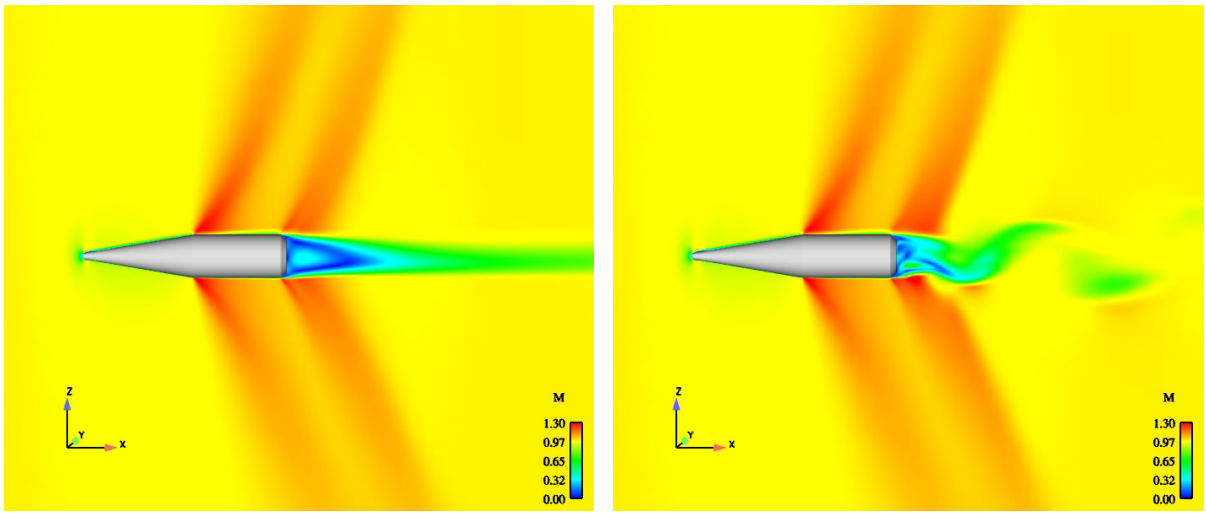

a) b)

Figure 14. Mach number contours on pitch plane at $M = 1.02$; (a) steady state k-ε-R and (b) time-accurate DES model.

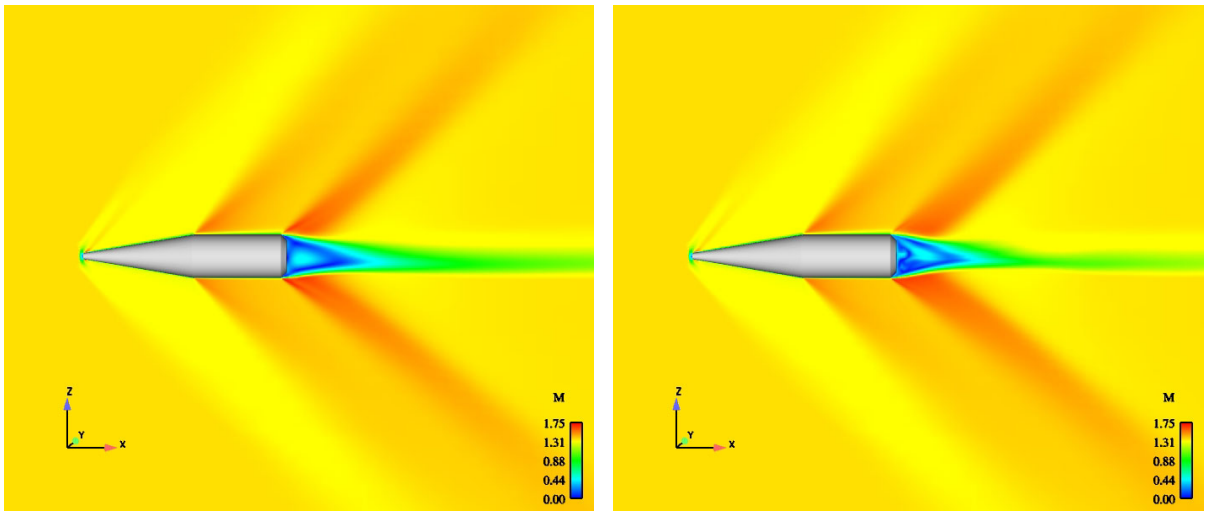

a) b)

Figure 15. Mach number contours on pitch plane at $M = 1.4$; (a) steady state k-ε-R and (b) time-accurate DES model.

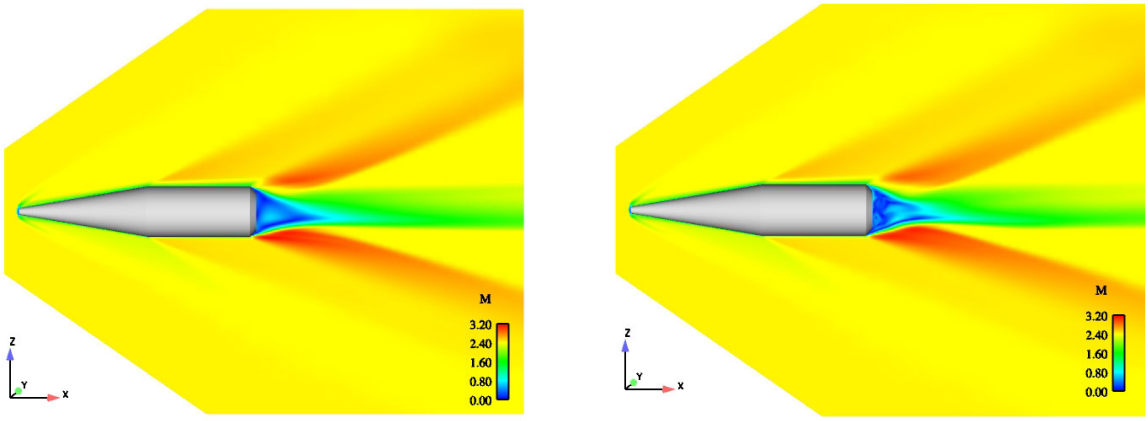

a) b)

Figure 16. Mach number contours on pitch plane at $M = 2.5$; (a) steady state k-ε-R and (b) time-accurate DES model.

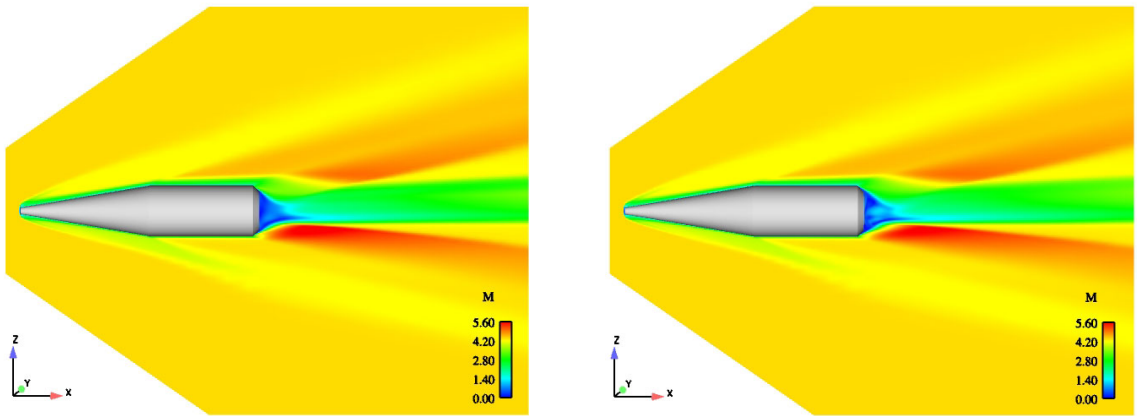

a) b)

Figure 17. Mach number contours on pitch plane at $M = 4.5$; (a) steady state k-ε-R and (b) time-accurate DES model.

IV. Conclusions

The CFD parameters necessary for the accurate prediction of the Magnus moment and roll damping of the M910 projectile were determined. Steady state calculations are adequate for the prediction of drag, normal (and lift) force, pitching moment, normal force center of pressure, and roll damping. Time-accurate, detached-eddy simulations were found necessary for the prediction of Magnus moment for $M < 2$. Steady state calculations appear adequate for $M > 2$. The k-ε-R turbulence model is recommended for steady state CFD calculations, as it provides the best convergence properties and most accurately predicts the roll damping (based on comparison with the DES calculations).

The CFD calculations can be performed in a reasonable time frame and are competitive with an experimental test program. This conclusion assumes that reasonable computational resources are available (e.g., 8–16 state-of-the-art processors). The requirement of a time-accurate calculation for Magnus moment is an issue, but the calculation is not required at all Mach numbers and angles of attack, thereby making the calculation viable.

Future work should quantify the differences in trajectory calculations, used to determine the ballistic match characteristics of the projectile, obtained by using aerodynamic coefficient data from the aeroballistic range, PRODAS predictions, and CFD predictions. Future work should also investigate the effects of different projectile base configurations on the accuracy of the CFD predictions. Does the chamfered base of the M910 projectile make it more or less difficult to obtain accurate CFD predictions? Archival experimental data exists for square base and boat tail base projectiles, which can be used for CFD validation.

Acknowledgments

This work was supported in part by a grant of high-performance computing time from the U.S. Department of Defense High Performance Computing Modernization program at the ARL Major Shared Resource Center, Aberdeen Proving Ground, Maryland.

References

[1]Sahu, J., DeSpirito, J., Edge, H. L., Silton, S. I., and Heavey, K. R., "Recent Applications of Structured and Unstructured Grid Techniques to Complex Projectile and Missile Configurations," *Eight International Grid Generation and Computational Field Simulations*, Honolulu, HI, June 2002.

[2]DeSpirito, J., Vaughn, M. E., Jr., and Washington, W. D., "Numerical Investigation of Canard-Controlled Missile Using Planar and Grid Tail Fins, Part I: Supersonic Flow," U.S. Army Research Laboratory, ARL-TR-2848, Aberdeen Proving Ground, MD, Sep. 2002.

[3]Sahu, J., Heavey, K. R., and Edge, H. L., "Numerical Computations of Supersonic Flow Over Elliptical Projectiles," U.S. Army Research Laboratory, ARL-TR-2589, Aberdeen Proving Ground, MD, Dec. 2001.

[4]Sahu, J., and Heavey, K. R., "Computational Fluid Dynamics Modeling of a 40-mm Grenade With and Without Jet Flow," U.S. Army Research Laboratory, ARL-TR-2572, Aberdeen Proving Ground, MD, Sep. 2001.

[5]Graham, M. J., Weinacht, P., Brandeis, J., and Angelini, R., "A Numerical Investigation of Supersonic Jet Interaction for Finned Bodies," U.S. Army Research Laboratory, ARL-TR-2312, Aberdeen Proving Ground, MD, Dec. 2000.

[6]Sahu, J., Heavey, K. R., Pressel, D., and Dinavahi, S., "Parallel Numerical Computations of Projectile Flow Fields," U.S. Army Research Laboratory, ARL-TR-2019, Aberdeen Proving Ground, MD, July 1999.

[7]Sahu, J., Edge, H. L., Heavey, K. R., and Ferry, E. N., "Computational Fluid Dynamics Modeling of Multi-body Missile Aerodynamic Interference," U.S. Army Research Laboratory, ARL-TR-1765, Aberdeen Proving Ground, MD, Aug. 1998.

[8]Silton, S. I., "Navier-Stokes Computations for a Spinning Projectile from Subsonic to Supersonic Speeds," U.S. Army Research Laboratory, ARL-TR-2850, Aberdeen Proving Ground, MD, Sep. 2002.

[9]Sturek, W. B., and Schiff, L. B., "Computations of the Magnus Effect for Slender Bodies in Supersonic Flow," *AIAA Journal*, Vol. 20, No. 12, 1982, pp. 1724–1731.

[10]Nietubicz, C. J., Sturek, W. B., and Heavey, K. R., "Computations of Projectile Magnus Effect at Transonic Velocities," U.S. Army Ballistic Research Laboratory, BRL-TR-02515, Aberdeen Proving Ground, MD, Aug. 1983.

[11]Sahu, J., "Transonic Navier-Stokes Computations for a Spinning Body of Revolution," U.S. Army Ballistic Research Laboratory, BRL-TR-3265, Aberdeen Proving Ground, MD, Sep. 1991.

[12]Plostins, P., McCoy, R. L., and Wagoner, B. A., "Aeroballistic Performance of the 25mm M910 TPDS-T Range Limited Training Projectile," U.S. Army Ballistic Research Laboratory, BRL-MR-3886, Aberdeen Proving Ground, MD, Jan. 1991.

[13]Arrow Tech Associates, "PRODAS Version 3 Technical Manual," South Burlington, VT, 2002.

[14]Oktay, E., and Akay, H. U., "CFD Predictions of Dynamic Derivatives for Missiles," AIAA-2002-0276, American Institute of Aeronautics and Astronautics, Jan. 2002.

[15]Park, S. H., Kim, Y., and Kwon, J. H., "Prediction of Damping Coefficients Using the Unsteady Euler Equations," *AIAA J. of Spacecraft & Rockets*, Vol. 40, No. 3, 2003, pp. 356–362.

[16]Park, S. H., and Kwon, J. H., "Navier-Stokes Computations of Stability Derivatives for Symmetric Projectiles," AIAA-2004-0014, American Institute of Aeronautics and Astronautics, Jan. 2004.

[17]Fluent, Inc., "Fluent 6.1 User's Guide," Vol. 2, Lebanon, NH, 2002.

[18]Metacomp Technologies, Inc., "CFD^{++} User's Manual," Agoura Hills, CA, 2002.

NO. OF
COPIES ORGANIZATION

1 (PDF ONLY) DEFENSE TECHNICAL INFORMATION CTR
DTIC OCA
8725 JOHN J KINGMAN RD
STE 0944
FORT BELVOIR VA 22060-6218

1 US ARMY RSRCH DEV & ENGRG CMD
SYSTEMS OF SYSTEMS INTEGRATION
AMSRD SS T
6000 6TH ST STE 100
FORT BELVOIR VA 22060-5608

1 DIRECTOR
US ARMY RESEARCH LAB
IMNE ALC IMS
2800 POWDER MILL RD
ADELPHI MD 20783-1197

3 DIRECTOR
US ARMY RESEARCH LAB
AMSRD ARL CI OK TL
2800 POWDER MILL RD
ADELPHI MD 20783-1197

ABERDEEN PROVING GROUND

1 DIR USARL
AMSRD ARL CI OK TP (BLDG 4600)

NO. OF COPIES ORGANIZATION

1 AEROPREDICTION INC
F MOORE
9449 GROVER DR STE 201
KING GEORGE VA 22485

1 UNIV OF TEXAS AT ARLINGTON
MECHL AND ARSPC ENGRG DEPT
J C DUTTON
BOX 19018
500 W FIRST ST
ARLINGTON TX 76019-0018

2 ATK TACTICAL SYSTEMS DIV
ALLEGANY BALLISTICS LAB
D J LEWIS
J S OWENS
210 STATE RT 956
ROCKET CENTER WV 26726

1 ATK ADVANCED WEAPONS DIV
R H DOHRN
MN06 1000
4600 NATHAN LANE N
PLYMOUTH MN 55442

1 ATK ORDNANCE SYS
B BECKER
MN07 MW44
4700 NATHAN LANE N
PLYMOUTH MN 55442

1 SCIENCE APPLICATIONS INTL CORP
J NORTHRUP
8500 NORMANDALE LAKE BLVD
STE 1610
BLOOMINGTON MN 55437

3 GOODRICH ACTUATION SYS
T KELLY
P FRANZ
J CHRISTIANA
100 PANTON RD
VERGENNES VT 05491

2 ARROW TECH ASSOC
W HATHAWAY
J WHYTE
1233 SHELBURNE RD STE D8
SOUTH BURLINGTON VT 05403

NO. OF COPIES ORGANIZATION

1 KLINE ENGRG CO INC
R W KLINE
27 FREDON GREENDEL RD
NEWTON NJ 07860-5213

1 GEORGIA INST TECH
DEPT ARSPC ENGR
M COSTELLO
270 FERST ST
ATLANTA GA 30332

1 AIR FORCE RSRCH LAB
AFRL/MNAV
G ABATE
101 W EGLIN BLVD STE 333
EGLIN AFB FL 32542-6810

1 US ARMY ARDEC
AMSRD AAR AEM A
G MALEJKO
PICATINNY ARSENAL NJ 07806-5000

1 US ARMY ARDEC
ASMRD AAR AEP E
D CARLUCCI
PICATINNY ARSENAL NJ 07806-5000

1 US ARMY ARDEC
ASMRD AAR AEP E
C KESSLER
PICATINNY ARSENAL NJ 07806-5000

1 US ARMY ARDEC
ASMRD AAR AEP E
I MEHMEDAGIC
PICATINNY ARSENAL NJ 07806-5000

1 PRODUCT MGR SMALL AND MED CALIBER AMMO
SFAE AMO MAS SMC
R KOWALSKI
BLDG 354
PICATINNY ARSENAL NJ 07806

1 PM MAS
SFAE AMO MAS
PICATINNY ARSENAL NJ 07806-5000

1 PM CAS
SFAE AMO CAS
PICATINNY ARSENAL NJ 07806-5000

NO. OF
COPIES ORGANIZATION

3 US ARMY AMRDEC
AMSAM RD SS AT
R W KRETZSHMAR
L AUMAN
E VAUGHN
REDSTONE ARSENAL AL 35898-5000

ABERDEEN PROVING GROUND

18 DIR USARL
AMSRD WM
J SMITH
AMSRD WM B
M ZOLTOSKI
J NEWILL
AMSRD WM BA
D LYON
AMSRD WM BC
P PLOSTINS
I CELMINS
M CHEN
J DESPIRITO (3 CPS)
B GUIDOS
K HEAVEY
J SAHU
S SILTON
P WEINACHT
AMSRD WM BD
B FORCH
AMSRD WM BF
S WILKERSON
H EDGE

NO. OF
COPIES ORGANIZATION

1 DSTL BEDFORD
T BIRCH
BLDG 115 RM 125
BEDFORD TECHNOLOGY PARK
BEDFORD
MK44 2FQ
UK

2 DEFENCE RESEARCH AND
DEVELOPMENT CANADA
VALCARTIER
F LESAGE
E FOURNIER
2459 PIE-XI BLVD NORTH
VAL BELAIR QC G3J1X5
CANADA